Periodically forced natural convection over slowly varying topography

By DUNCAN E. FARROW

Mathematics and Statistics, Division of Science and Engineering, Murdoch University,
Murdoch, WA 6150, Australia

Asymptotic and numerical methods are used to analyse periodically forced natural convection over slowly varying topography. This models the diurnal heating/cooling cycle in lakes and reservoirs. The asymptotic solution includes the effects of advection on the temperature. The asymptotic results are confirmed by the numerical results. The numerical results are also used to examine flow regimes where the asymptotic results break down. In particular, the presence of a vertical boundary leads to a permanent stratification in the deeper regions due to a nonlinear pumping process in the shallows. Heat transfer calculations and two limiting cases are also presented.

1. Introduction

Fluid motion driven by temperature-induced horizontal density gradients is an important part of the dynamics of lakes and other geophysical fluid bodies. There are a number of ways that horizontal density gradients can be be generated. For example, if a spatially uniform surface heat flux is distributed over the local depth in a lake or reservoir then the shallower regions will heat up more rapidly than the deeper parts. Simple scaling for flow in typical lake or reservoir (Monismith, Imberger & Morison 1990) shows that the time for adjustment to a change in the forcing is typically much longer than a day. In the case where the main thermal forcing is the diurnal heating/cooling cycle this means that the flow is never in equilibrium with the forcing. One consequence of this is that the circulation in a reservoir sidearm or the littoral region of a lake will not be in phase with the thermal forcing; the flow will be against the prevailing pressure gradient (Farrow & Patterson 1993, hereafter referred to as FP93). This has been observed in natural lakes by Monismith *et al.* (1990) and Adams & Wells (1984).

Geophysical flows have motivated a number of investigations into low-aspect-ratio rectangular cavities. The classic cubic velocity profile for the steady-state convection in a long box driven by a density gradient was apparently first derived by Rattray & Hansen (1962). Hart (1972) showed that this profile was an exact solution for the flow driven by a density gradient between two parallel infinite plates. Steady convection in a long box with differentially heated endwalls was considered by Cormack, Leal & Imberger (1974). There have been a number of studies since then based on steady flow in a shallow rectangular cavity.

The rectangular cavity is not an adequate model for many geophysical situations where variable (or sloping) bathymetry has a significant effect on the system. For example Horsch, Stefan & Gavali (1994) considered the flow down the slope of the littoral region of a lake due to nighttime surface cooling. Farrow & Patterson (1994)
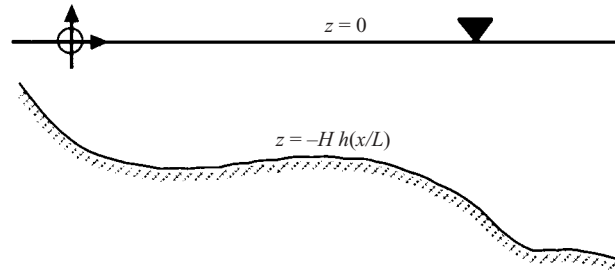
FIGURE 1. Schematic of the flow domain showing the coordinate system and definition of bathymetry.

considered the corresponding flow during daytime heating. More recently, Lei & Patterson (2002) conducted a detailed scaling of the daytime heating problem. All of these studies rely on a sloping bottom boundary to drive a general circulation. Sturman, Oldham & Ivey (1999) built on Horsch *et al.*'s (1994) work, considering the exchange flow between a cooled littoral region and the main water body. Convection in a variable-depth cavity has also been considered by Poulikakos & Bejan (1983) where they modelled the fluid motion in an attic space.

All the above studies include either steady-state conditions or steady forcing. However, as mentioned earlier, the response time of a typical lake is longer than a day. Thus there is one feature of the diurnally forced case that is not included in the above studies: the response to unsteady forcing. FP93 report lowest-order asymptotic and limited numerical solutions for an idealized reservoir sidearm with a triangular geometry. They included periodic (in time) thermal forcing modelling the diurnal cycle. They found that the response could be divided into a shallow region where the flow is in a viscous/buoyancy balance (so the circulation response was in phase with the prevailing pressure gradient) and a deeper region where the flow is in an unsteady inertia/buoyancy balance (so the circulation response lagged the pressure forcing).

This paper also considers flows driven by differential heating/cooling associated with variable topography and the diurnal cycle, building on the results of FP93. The generalizations here include arbitrary bathymetry, higher-order asymptotic results and a more comprehensive set of numerical simulations. The numerical simulations allow an investigation of regions of parameter space where the asymptotic results do not provide an adequate description of the flow. Extra physics that emerge from the numerical results include the formation of warm surface and cool bottom currents, the setting up of permanent stratification by advection in the shallows and a 'filling box' mechanism leading to stratification of the deeper regions.

The structure of the paper is as follows. A model for periodically forced natural convection is formulated in §2. An asymptotic solution for the model is found in §3 based on a small characteristic bottom slope. The validity of the asymptotic solution is limited, which motivates the numerical simulations of the full model in §4. The results of the asymptotic and numerical results are discussed in §5. Finally, general conclusions and suggestions for further work are given in §6.

2. Model formulation and non-dimensionalization

Figure 1 shows a schematic of the model domain. The variable topography is modelled as $z = -Hh(x/L)$ where H is a scale for the depth and L is a scale for the horizontal variability of the topography. The function $h(.)$ is arbitrary; however

it is assumed to be continuous and have bounded derivatives. It will be assumed later that $A = H/L$ (a scale for the bottom slope) is small. The periodic forcing is modelled by an internal heating/cooling term in the heat equation. Following FP93 the internal heating term is formulated by taking a periodic uniform surface heat flux $I_0 \cos(2\pi t/P) \, \text{W m}^{-1}$, where P is the period of the heating (that is 24 hours), and distributing it uniformly over the local depth. This choice of the source term means that $t = 0$ corresponds to midday, i.e. when the heating is at its most intense. This ensures that there is a reversal of the pressure gradient during the diurnal cycle.

The uniform vertical distribution of the source term is a considerable simplification of the heating/cooling mechanisms that occur in natural lakes. For example, during the day heating occurs mainly near the surface which, in the absence of significant mixing, leads to a significant vertical structure in the temperature, especially in the deeper regions. The uniform cooling assumption is more reasonable as surface cooling will generally generate thermals distributing the heat flux over the local depth. However, it is difficult to make analytical progress with more general thermal models although the unsteady daytime heating case has been considered by Farrow & Patterson (1994) and Lei & Patterson (2002). The focus of the present work is on the general circulation induced by differential heating and cooling due to topographic effects. A vertically uniform heating/cooling model is adequate for this purpose. Also, including more general heating/cooling mechanisms generates further modelling issues that are beyond the scope of the present work.

With the above assumptions and the Boussinesq approximation the equations of motion are

$$\frac{\mathrm{D}u}{\mathrm{D}t} = -\frac{1}{\rho_0}\frac{\partial p}{\partial x} + \nu\nabla^2 u, \tag{2.1}$$

$$\frac{\mathrm{D}w}{\mathrm{D}t} = -\frac{1}{\rho_0}\frac{\partial p}{\partial z} + \nu\nabla^2 w + g\alpha(T - T_0), \tag{2.2}$$

$$\frac{\mathrm{D}T}{\mathrm{D}t} = \kappa\nabla^2 T + \frac{I_0 \cos(2\pi t/P)}{\rho_0 C_p H h(x/L)}, \tag{2.3}$$

$$u_x + w_z = 0, \tag{2.4}$$

where u and w are the horizontal and vertical velocities, p is the pressure perturbation, T is the temperature, T_0 is the reference temperature, ρ_0 is the reference density, ν is the viscosity, κ is the thermal diffusivity, g is acceleration due to gravity, α is the thermal expansion coefficient and C_p is the specific heat of water. It is assumed here that ν and κ are constant; however it is possible to have separate vertical and horizontal eddy diffusivities and still make analytical progress.

It is assumed that all heat input/output is accounted for by the internal heating term so all boundaries are taken to be insulated. Also, the bottom boundary $z = -Hh(x/L)$ is taken to be rigid and impermeable and the upper boundary $z = 0$ is not disturbed and stress free. These assumptions lead to the boundary conditions

$$u_z = 0, \quad w = 0, \quad T_z = 0 \quad \text{on} \quad z = 0, \tag{2.5}$$
$$u = w = 0, \quad Ah'T_x + T_z = 0 \quad \text{on} \quad z = -Hh(x/L). \tag{2.6}$$

At $t = 0$ when the heating is turned on, it is assumed that the fluid is isothermal and at rest: $T = T_0$ and $u = w = 0$ at $t = 0$.

Before analysing this model, the system of equations is non-dimensionalized. The general geometry of the domain imposes no natural lengthscale. However, there is a natural timescale for this model: $t \sim \tau = P$, the period of the forcing. From

this, a vertical length can be constructed by considering the growth of a viscous boundary layer at the near-horizontal rigid bottom boundary. This layer will grow in thickness like $\sqrt{\nu t}$. Letting $t = \tau$ yields a vertical lengthscale $z \sim H = \sqrt{\nu P}$. The physical interpretation of this lengthscale is that it is the thickness to which a viscous boundary layer will grow during one period of the diurnal forcing. If A is a scale for the bottom slope of the domain then an appropriate horizontal lengthscale is $x \sim L = H/A$.

Balancing the unsteady and internal heating terms in the temperature equation yields a scale for the temperature: $T - T_0 \sim I_0 P/(\rho_0 C_p \sqrt{\nu P})$. Assuming a hydrostatic balance and balancing unsteady inertia with the horizontal pressure gradient yields pressure and horizontal velocity scales $p \sim g\alpha I_0 P/C_p$ and $u \sim AGr\sqrt{\nu/P}$ where Gr is the Grashof number given by

$$Gr = \frac{g\alpha \Delta T_0 H^3}{\nu^2} = \frac{g\alpha I_0 P^2}{\rho_0 C_p \nu}. \tag{2.7}$$

Finally, the continuity equation yields a scale for the vertical velocity $w \sim A^2 Gr\sqrt{\nu/P}$.

Typical field values can calculated using the parameters of Monismith et al. (1990). Using $I_0 = 10^3 \, \mathrm{W\,m^{-2}}$ and the usual values for the other parameters gives the Grashof number ranging from $Gr \approx 10^7$ for an eddy viscosity of $\nu = 10^{-4}$ to $Gr \approx 10^9$ for molecular values of ν. A typical bottom slope A ranges from 10^{-3} to 10^{-2}.

The non-dimensional equations governing this system are then

$$u_t + A^2 Gr(uu_x + wu_z) = -p_x + A^2 u_{xx} + u_{zz}, \tag{2.8}$$

$$w_t + A^2 Gr(wu_x + ww_z) = -p_z/A^2 + A^2 w_{xx} + w_{zz} + T/A^2, \tag{2.9}$$

$$T_t + A^2 Gr(uT_x + wT_z) = \frac{1}{\sigma}(A^2 T_{xx} + T_{zz}) + \frac{1}{h(x)}\cos(2\pi t), \tag{2.10}$$

$$u_x + w_z = 0, \tag{2.11}$$

where $\sigma = \nu/\kappa$ is the Prandtl number and all variables are now non-dimensional. The boundary conditions become

$$u_z = w = T_z = 0 \quad \text{on} \quad z = 0, \tag{2.12}$$

$$u = w = A^2 h' T_x + T_z = 0 \quad \text{on} \quad z = -h(x), \tag{2.13}$$

and the initial conditions are $u = w = T = p = 0$.

3. Asymptotic solution

The system of equations (2.8)–(2.11) does not admit an analytical solution. However, asymptotic solutions based on $A \ll 1$ can be found. The technique is similar to that of Cormack, Stone & Leal (1974), Poulikakos & Bejan (1983) and FP93. The horizontal velocity is expanded in the form

$$u(x, z, t) = u^{(0)}(x, z, t) + A^2 u^{(2)}(x, z, t) + \cdots,$$

with similar expansions for the other dependent variables. The solution procedure consists of substituting these expansions into the equations above and then equating like powers of A. The resulting system of linear equations can then be solved recursively starting with the zeroth order in A. Each of these equations is a linear PDE with z and t being the independent variables. The horizontal variable becomes a parameter determining the local conditions (through $h(x)$ and its derivatives). Even though each equation in this system is linear the algebraic complexity increases

dramatically as the order increases. Thus, only the $O(A^0)$ solution for u and the $O(A^2)$ solution for T are found here.

3.1. *Zero-order temperature*

The $O(A^0)$ temperature equation expresses a simple balance between the internal heating and the unsteady term. The boundary conditions are $T_z^{(0)} = 0$ on $z = 0,\ -h$. The solution is then

$$T^{(0)} = \frac{1}{2\pi h(x)}\sin(2\pi t). \tag{3.1}$$

This solution appears as a forcing term in the horizontal momentum equation at zero order and has period 1. Note that the heating is proportional to $\cos(2\pi t)$ while $T^{(0)}$ is proportional to $\sin(2\pi t)$.

3.2. *Zero-order velocity*

The zero-order horizontal velocity equation is

$$u_t^{(0)} = -p_x^{(0)} + u_{zz}^{(0)} \tag{3.2}$$

with boundary conditions $u_z^{(0)} = 0$ on $z = 0$ and $u^{(0)} = 0$ on $z = -h$. Physically, the unsteady temperature field induces a hydrostatic pressure field that drives a circulation.

The solution procedure for this equation involves eliminating the pressure and recasting the problem in terms of a streamfunction. The details are omitted; however the solution for the horizontal velocity is

$$
\begin{aligned}
u^{(0)} = &-\frac{h'}{96\pi h^2}\sin(2\pi t)(z+h)(8z^2 + zh - h^2)\\
&- 2h'h\sum_{n=1}^{\infty}\frac{\cos\beta_n + (\cos\beta_n - 1)/\beta_n^2 - \frac{1}{2}}{\beta_n^3\sin\beta_n\left(\alpha_n^4 + (2\pi)^2\right)}(\cos(\alpha_n z) - \cos\beta_n)\\
&\times \left(\alpha_n^2\left(\cos(2\pi t) - \exp\left(-\alpha_n^2 t\right)\right) + 2\pi\sin(2\pi t)\right)
\end{aligned}
\tag{3.3}
$$

where β_n are the positive roots of the equation $\beta_n = \tan\beta_n$ and $\alpha_n = \beta_n/h$. The first term of this solution can be obtained by assuming a viscous/buoyancy balance in (3.2) and is the same (up to multiplication by a function of x and t) as that found in Cormack *et al.* (1975).

3.3. *Second-order temperature*

The $O(A^2)$ temperature equation is

$$T_t^{(2)} = \frac{1}{\sigma}T_{zz}^{(2)} + \frac{1}{\sigma}T_{xx}^{(0)} - Gr u^{(0)}T_x^{(0)}. \tag{3.4}$$

This equation is a standard one-dimensional heat equation with two forcing terms. The first of these represents a correction for horizontal conduction which is not included in the $O(A^0)$ solution and the second term represents advection of $T^{(0)}$ by $u^{(0)}$. There is no contribution from vertical advection since $T^{(0)}$ is independent of z. The boundary conditions on $T^{(2)}$ are

$$T_z^{(2)} = 0 \qquad \text{on} \quad z = 0, \tag{3.5}$$

$$T_z^{(2)} = -h'T_x^{(0)} \qquad \text{on} \quad z = -h. \tag{3.6}$$

The second of these boundary conditions is a correction to account for the non-zero slope of the bottom boundary. The forcing terms involve infinite series which in turn lead to a doubly infinite series solution for $T^{(2)}$. The solution is given in the Appendix.

3.4. Advective heat transfer

The horizontal advective heat transfer per unit width is given by (in terms of dimensionless variables)

$$Q = AGr\, I_0(\nu P)^{1/2} \int_{-h}^{0} uT\, dz \quad \text{W m}^{-1}. \tag{3.7}$$

The total heat transfer includes a conduction component which is negligible for the small-A case considered here. In terms of the asymptotic solution above

$$Q = AGr\, I_0(\nu P)^{1/2} q + O(A^5) \tag{3.8}$$

where

$$q = A^2 \int_{-h}^{0} u^{(0)} T^{(2)}\, dz. \tag{3.9}$$

The zero-order temperature $T^{(0)}$ does not contribute to Q since it is independent of z.

3.5. Limiting cases

The asymptotic solutions given above include both unsteady inertia and viscous effects. Neglecting one or other of these effects gives two limiting cases representing either the viscous- or inertia-dominated case. Note that $T^{(0)}$ is the same for both cases. Neglecting viscous and diffusive effects gives

$$u_i^{(0)} = \frac{h'}{4\pi^2 h}\left(\frac{z}{h}+\frac{1}{2}\right)(1-\cos(2\pi t)) \tag{3.10}$$

and

$$T_i^{(2)} = \frac{Gr(h')^2}{64\pi^4 h^3}\left(\frac{z}{h}+\frac{1}{2}\right)(3-4\cos(2\pi t)+\cos(4\pi t)). \tag{3.11}$$

Note that neither $u_i^{(0)}$ nor $T_i^{(2)}$ satisfy the boundary conditions at the top and bottom of the domain. This is a consequence of neglecting viscosity and diffusion. The only extra physics included in $T_i^{(2)}$ is the advection of $T^{(0)}$ by $u_i^{(0)}$. The horizontal advective heat transfer corresponding to the inviscid limit is

$$q_i = \frac{A^2 Gr(h')^3}{6,144\pi^6 h^3}(10-15\cos(2\pi t)+6\cos(4\pi t)-\cos(6\pi t)). \tag{3.12}$$

Neglecting unsteady inertia effects (and assuming diffusion dominates the heat equation) yields

$$u_\nu^{(0)} = -\frac{h'h}{96\pi}\left(\frac{z}{h}+1\right)\left(8\left(\frac{z}{h}\right)^2+\frac{z}{h}-1\right)\sin(2\pi t) \tag{3.13}$$

and

$$T_\nu^{(2)} = \frac{(h')^2-hh''}{4\sigma\pi^2 h^3}(1-\cos(2\pi t))-\frac{(h')^2}{4\pi h}\left(\left(\frac{z}{h}\right)^2-\frac{1}{3}\right)\sin(2\pi t)$$
$$+\frac{Gr\sigma(h')^2 h}{23,040\pi^2}\left(24\left(\frac{z}{h}\right)^5+45\left(\frac{z}{h}\right)^4-30\left(\frac{z}{h}\right)^2+5\right)(1-\cos(4\pi t)). \tag{3.14}$$

Note that $u_\nu^{(0)}$ is simply the first term of (3.3). The solution of $T_\nu^{(2)}$ includes three terms which represent respectively: a correction for horizontal conduction, a correction to account for the sloping bottom (isotherms must be normal to the bottom) and

advection of $T^{(0)}$ by $u^{(0)}$. The advection correction term has the same form as the steady solution of Cormack *et al.* (1975). Only the last two terms contribute to the horizontal advective heat transfer in this limit, which is given by

$$q_v = \frac{A^2 (h')^3 h}{5,760\pi^2}(1 - \cos(4\pi t)) + \frac{19 A^2 Gr\sigma (h'h)^3}{92,897,280\pi^3}(3\sin(2\pi t) - \sin(6\pi t)). \quad (3.15)$$

4. Numerical solution

The asymptotic solution described above is only valid in a restricted region of parameter space. Specifically, it requires A^2 and $A^2 Gr$ to be small. While the first of these constraints is generally true for lakes the second is not. A numerical solution of the full equations allows an examination of the parameter regime where the asymptotic solution breaks down as well as validating the asymptotic solution where it is expected to adequately describe the system.

For the numerical solution a linear bottom profile is assumed, i.e. $h(x) = x$. This allows the governing equations to be recast into polar coordinates (r, θ) with the upper and lower boundaries lying on coordinate lines. Extra boundaries need to be added near the tip $x = 0$ (at $r = r_{min}$) and at some distance from the tip (at $r = r_{max}$) to keep the computational domain finite. The extra boundary at $r = r_{min}$ is necessary to allow the timestep to be sufficiently large without violating stability constraints (see below). These near-vertical boundaries are not present in the model formulation above so extra boundary conditions need to be specified. The temperature gradient at each of these boundaries is set to match that of the zero-order solution above. The boundaries are also taken to be rigid and non-slip. An alternative approach would be to have open boundary conditions at $r = r_{min}$ and $r = r_{max}$. This would mean the numerical model would be closer to the analytical model above. However, such boundary conditions cannot be achieved in the laboratory and the extra physics associated with rigid boundary conditions is of interest.

The numerical method is a SIMPLE type scheme on a non-staggered mesh with Leonard's (1979) QUICK correction. The details of the method can be found in Armfield (1991) and Farrow (1995). A number of simulations have been carried out using different A, Gr and r_{max}. The non-uniform grid is typically 225×53 (for $r_{max} = 6$) with extra points near solid boundaries to resolve viscous boundary layers. There is a diffusive limit on the timestep set by the converging coordinate lines near $x = 0$ which restricts the choice of both the position of the boundary there and the timestep. In the simulations presented here, $r_{min} = 0.4$ and the timestep is 2.5×10^{-5}. All simulations here use $\sigma = 7$.

5. Discussion

5.1. *Preliminary remarks*

The asymptotic solutions in §3 allow for general topography. The discussion here concentrates on the particular case $h(x) = x$, i.e. a triangular domain with a constant bottom slope. This is also the topography used in the numerical simulations. The flow development, at least for small A, is qualitatively the same for other topographies. The asymptotic solutions depend principally on h and h'. The second derivative of h appears only in the horizontal-conduction correction part of $T^{(2)}$ and thus plays a minor role in the physics contained in the asymptotic solutions.
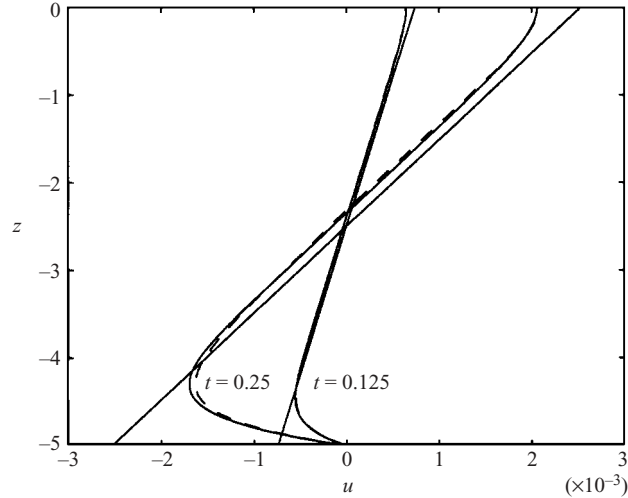
D. E. Farrow

FIGURE 2. Horizontal velocity profiles at $x = 5$ at small times from the analytical (solid) and numerical (dashed) results for $A = 0.1$, $Gr = 10^4$ and $r_{max} = 6$. The straight lines are calculated assuming a pure inertia balance.

It was pointed out in FP93 that for $h = x$ the asymptotic solution fails near $x = 0$. This is because the horizontal diffusion term in (2.10) cannot be ignored as $x \to 0$. However, the region where horizontal diffusion is important is generally small. Using the zero-order temperature to estimate the ratio of $A^2 T_{xx}/T_t$ shows that horizontal diffusion is only important for $x < A$ (FP93), which represents a very small part of the domain of interest.

FP93 discuss in detail the behaviour of this system in the linear regime and their results are summarized below. The discussion here concentrates on the additional dynamics associated with nonlinear effects and the presence of the endwall at the deep end of the domain.

5.2. *The linear regime*

The heating of the isothermal quiescent fluid begins at $t = 0$ which corresponds to midday in the diurnal cycle. As heat is added to the system a horizontal pressure gradient (proportional to $\sin 2\pi t$) is established which favours a clockwise (daytime) circulation. This circulation is initially in an inertia/buoyancy balance and is represented well by (3.10). Note that $u_i^{(0)}$ has a linear profile and does not satisfy the upper and lower boundary conditions. Also, $u_i^{(0)} \propto t^2$ for small t and is unbounded as $x \to 0$. Figure 2 shows a number of velocity profiles at early times for $h = x$ at $x = 5$ from the asymptotic and numerical results for $A = 0.1$ and $Gr = 10^4$. Also included in that figure are the linear velocity profiles predicted by a pure inertia/buoyancy balance. The agreement between the numerical and asymptotic results is excellent. Away from the upper and lower boundaries, the results are also in agreement with the inertia/buoyancy solution (3.10). There is a slight offset due to the asymmetry of the boundary conditions. The velocity profiles diverge from linear near the upper and lower boundaries where there are viscous boundary layers. The divergence is more obvious near the lower boundary where there is a no-slip boundary condition. These boundary layers grow in thickness like $t^{1/2}$ (in dimensionless variables). Eventually, the thickness of the boundary layers will be of the same order as the local depth. The time this takes depends on the local depth and is given by $t_\nu \sim x^2$. Mathematically,

this is the e-folding time of the exponential terms in (3.3). Since the thickness of the boundary layers is independent of the local depth there is always a region near $x = 0$ where the local depth is less than the boundary layer thickness. Specifically, for $x < t^{1/2}$ the boundary layers encompass the entire local depth. For $x \ll 1$, the flow will be in a viscous/buoyancy balance in a time much shorter than the diurnal period. For $x \ll 1$, the velocity profile is represented well by a viscous/buoyancy balance which is represented by the first term of (3.3). In this region $u^{(0)} \propto t$ for small t and $u^{(0)} \to 0$ as $x \to 0$.

In the absence of pronounced nonlinear effects, the established flow can be divided into three regions (FP93): a shallow ($x < 1$) viscous-dominated region where the circulation is in phase with the pressure-gradient forcing, a deep ($x > 1$) inertia-dominated region where the circulation lags the forcing by one quarter of a period, and an intermediate ($x \sim 1$) region where the lag depends strongly on x. Over the course of a diurnal cycle, the circulation in each region changes sign. In the shallow viscous region the reversal happens nearly simultaneously over the entire depth. The reversal in the transitional and inertia-dominated region is more complex. The pressure gradient reverses simultaneously over the entire depth. The flow near the rigid bottom boundary is dominated by viscous effects and is the first to respond to the reversed pressure gradient. The interior inertia-dominated flow responds more slowly. This leads to a complex circulation pattern as the flow reverses, with multilayer flow (FP93).

Note that $u \to 0$ as $x \to 0$, $x \to \infty$ and $t \to 0$. The linear results apply in each of these limits. The range of validity of the linear results can be calculated by requiring that terms omitted from the governing equations should be smaller than those that are included. The maximum u is $U \approx 5 \times 10^{-3}$. For $x \to 0$, the main balance is between buoyancy and vertical shear which gives $x < 200/(A^2 Gr)$ as the linear region. For $x \to \infty$, the main balance is between buoyancy and inertia which gives $x > A^2 Gr/200$. Combining these two results gives $A^2 Gr < 200$ for the flow in the entire domain to be linear. Given the typical values for natural lakes given above, this condition is not generally met in many natural lakes although there will be some regions where the linear results will hold.

5.3. *Nonlinear effects*

As mentioned above, the asymptotic solution relies on small A^2 and small $A^2 Gr$. The second of these parameters is generally not small in natural lakes and represents the importance of nonlinear effects (specifically advection) in the physics. From the point of view of the initial value problem considered here, the first effect to emerge is advection of temperature.

Figure 3 shows a series of snapshots of the temperature and streamfunction contours at various times from the asymptotic results for $A = 0.1$ and $Gr = 10^4$. The effect of advection on the temperature is evident from the tilting of the isotherms in figure 3(a–e). In each case, advection has tilted the isotherms so as to set up a stable (albeit weak) stratification. The corresponding circulation is shown in figure 3(f–j). Note that the asymptotic circulation shown here is driven entirely by the zero-order temperature (3.1). The forcing due to the zero-order temperature changes sign at $t = 0.5$ (figure 3b, g) and $t = 1$ (figure 3d, i). At these times there is stable stratification that was set up prior to the reversal of the pressure gradient. Even though the pressure gradient driving the zero-order circulation vanishes at $t = 0.5$ and $t = 1$ there is still a substantial circulation in the deeper parts of the domain due to the inertia of the existing flow. By $t = 0.75$, the pressure gradient has reversed the flow in the shallows and in the bottom boundary layer (figure 3h) but there is still a region of clockwise circulation in the interior.
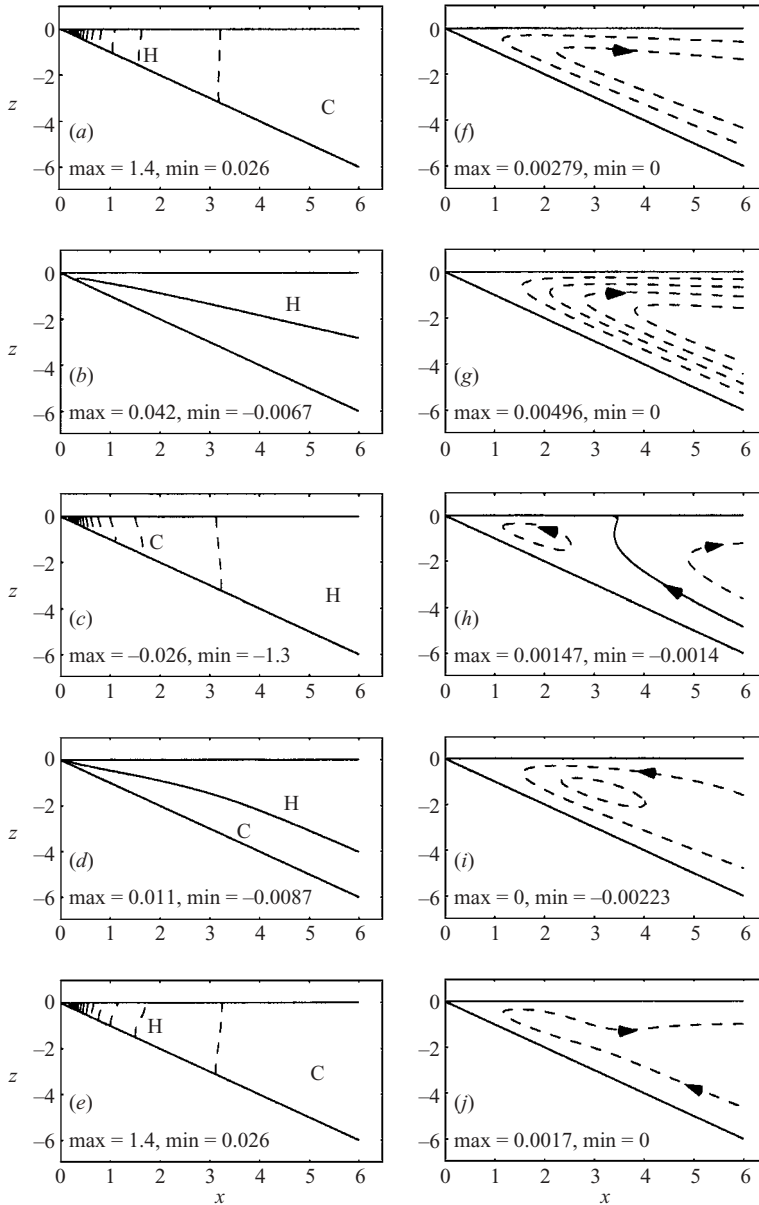
FIGURE 3. Series of snapshots of $(a-e)$ temperature and $(f-j)$ streamfunction from the asymptotic solution for $h = x$. The contour intervals are for $(a-e)$ 0.005 and for $(f-j)$ 0.001. Here, $A = 0.1$ and $Gr = 10^4$. The solid contour is the zero contour and the 'C' and 'H' symbols indicate relatively cold and hot fluid respectively. (a, f) $t = 0.25$; (b, g) $t = 0.5$; (c, h) $t = 0.75$; (d, i) $t = 1$; (e, j) $t = 1.25$.

Figure 4 show a series of snapshots of the temperature and streamfunction contours for the same parameter and times as figure 3 but now using the numerical results. The two sets of results are generally in very good agreement except near the two endwalls that are not present in the asymptotic results. The circulation is turned around in a region near the endwall of width $Ar_{max} = 0.6$. This region will be dominated by
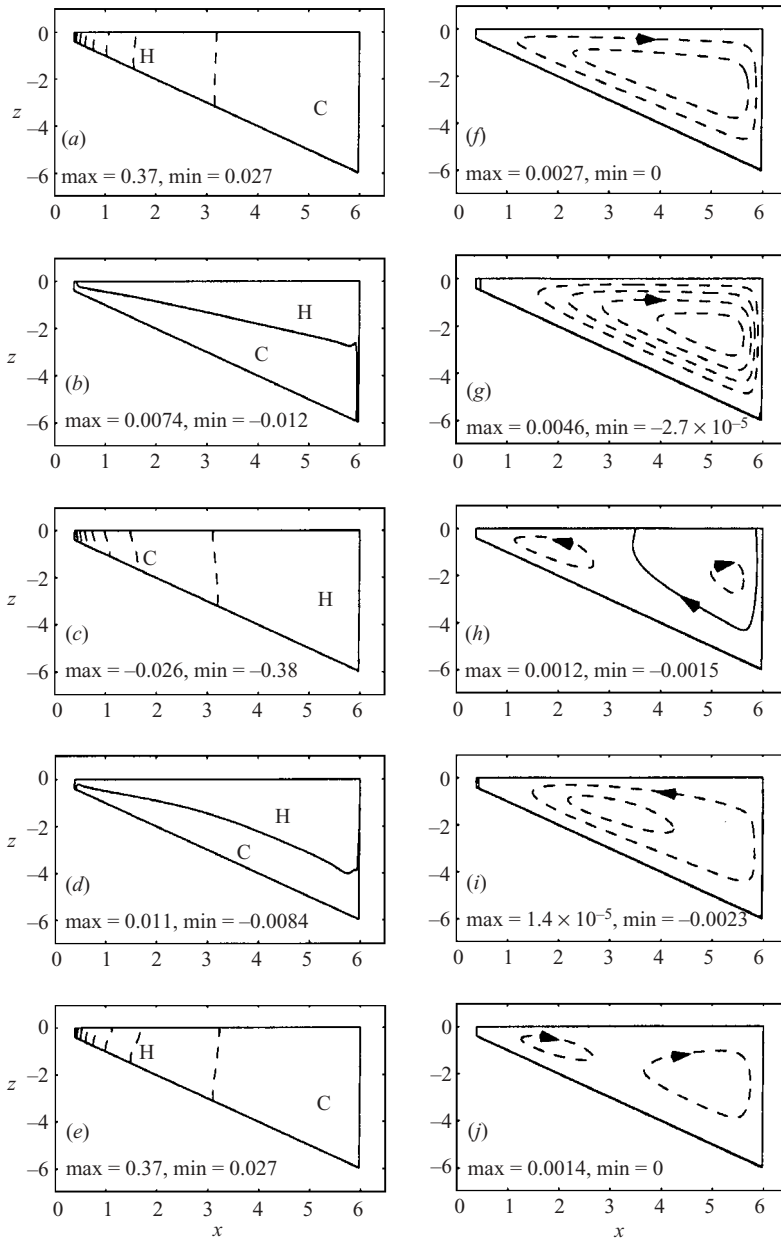
FIGURE 4. As for figure 3 but now using numerical results with $r_{max} = 6$.

viscous effects which can be seen in figure 4(*h*) where the circulation reverses first in response to a change in sign of the pressure gradient both in the shallows and near the endwall. Note that the circulation magnitudes in the numerical results are slightly smaller than for the asymptotic results (up to about 5% smaller in the shallows). This is due to horizontal conduction (which is not included in the asymptotic results) weakening the background temperature gradient in the numerical results.

The inclusion of nonlinear effects in the asymptotic solutions permits estimation of horizontal advective heat transfer. This is zero at $O(A^0)$ since $T^{(0)}$ is independent of
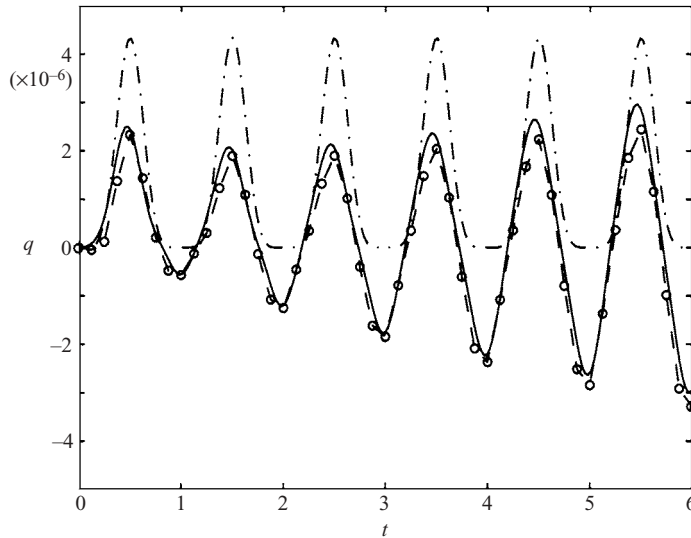
FIGURE 5. Time series of the horizontal advective heat transfer at $x = 5$ from the analytical (solid), numerical (dashed with circles) and pure inertia (dot-dashed) results for the same parameters as figure 3.

depth. Figure 5 shows a time series of the horizontal advective heat transfer at $x = 5$ from the numerical and asymptotic results. Also included is the asymptotic result q_i with viscous and diffusive effects neglected. As discussed above, for small times the initial balance is between inertia and buoyancy. If this balance were maintained, the heat transfer would never be negative, as indicated by q_i. This is because there is no reversal of the circulation in the inertia-dominated regime. There is a reversal of the background temperature gradient $T^{(0)}$; however this does not give rise to a reversal of $T^{(2)}$ as the time dependent term in (3.11) is greater than or equal to zero for all $t \geqslant 0$.

The agreement between the full asymptotic solution and the numerical solution is very good for the times shown in figure 5. There is some discrepancy due to processes, such as horizontal conduction, that are not included in the asymptotic solution. Also, at $x = 5$ the presence of the endwall at $r = 6$ is having some effect on the numerical results. For small times, the asymptotic and numerical results are in general agreement with the inviscid solution q_i. However, the results diverge quite quickly and by $t = 0.5$, q_i has about twice the magnitude of the other results. This is due to the growth of viscous boundary layers at the top and (especially) bottom of the domain. In the inviscid solution (3.10)–(3.11) the greatest contribution to q_i occurs at the top and bottom of the domain. These two regions are also the first to feel the effects of viscosity. Whereas in the inviscid solutions the maximum $u_i^{(0)}$ and $T_i^{(2)}$ occur at $z = -h$, for the full solution $u^{(0)} = 0$ at $z = -h$. At $x = 5$, the time to reach the established (periodic) flow is $t \sim 10$. However, the flow by $t = 4$ is close to periodic with just a general increase in magnitude. Note that for $x = 5$, q_v is over 300 times larger than q_i. Thus q_i provides a better estimate of the magnitude of q but it does not take into account the effect of the boundary layer growth. Even though the flow is dominated by the effects of inertia in the sense that the general circulation lags the forcing, the heat transfer is strongly influenced by viscous effects.

Figure 6 shows a time series of the horizontal advective heat transfer at $x = 1$ from the asymptotic and numerical results. Also included is the viscous limit q_v for
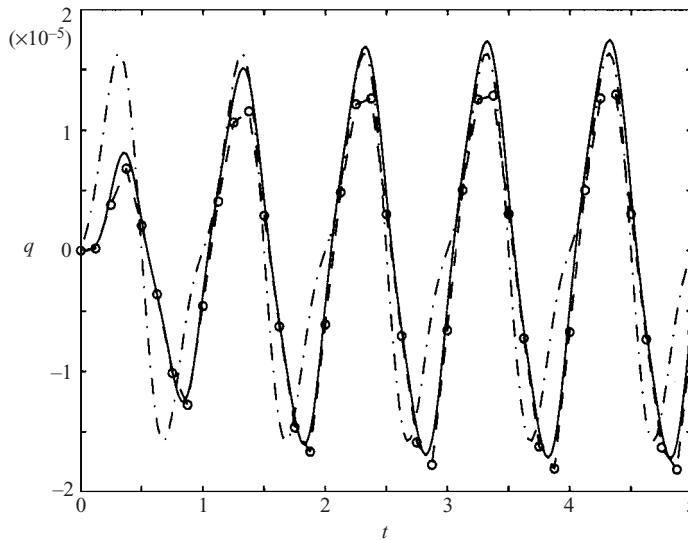
FIGURE 6. Time series of the horizontal advective heat transfer at $x = 1$ from the analytical (solid), numerical (dashed with circles) and viscous-dominated (dot-dashed) results for the same parameters as figure 3.

comparison. Even at $x = 1$, there are some inertia effects at small times. However, by $t = 2$, an established periodic structure has emerged which agrees remarkably well with the viscous-dominated result. Note that at $x = 1$ and with these parameter values, the main contribution to q_v is from the second term in (3.15). In the viscous regime the advection correction term of q_v (the term proportional to Gr) has extrema at $t = n \pm 1/4$. This corresponds precisely with the extrema of $u_v^{(0)}$ as would be expected since the viscous-dominated regime can be viewed as a modulated steady state. Both the asymptotic and numerical results slightly lag q_v due to the effects of inertia.

5.4. *Effects of the endwall*

There is a near vertical solid wall at $r = r_{\max}$ in the numerical results that is not present in the asymptotic results. The presence of the endwall introduces additional physical effects that are not and cannot be captured by the asymptotic results above. Mathematically, the derivatives of $h(x)$ are no longer bounded. The first feature to appear is a viscous boundary layer on the endwall where streamlines emerging from the interior flow close (streamlines continue to infinity in the asymptotic model, see figure 3). For small A, the effect of the endwall is limited to a region of width $Ar_{\max}$, at least for small times. In this case, the endwall region is akin to the end regions in the steady-state solutions of Cormack *et al.* (1974). In that work the core flow was driven by thermal boundary conditions on the vertical walls. This meant that it was necessary to solve for the flow in the end regions. This is not necessary here since the flow is driven by a pressure gradient induced by the thermal forcing interacting with the topography.

A more interesting effect of the endwall that leads to a significant modification of the flow in the interior of the cavity occurs when the flow is nonlinear. If advection is sufficiently strong a slug of warm water will emerge from the shallows during the initial heating phase. This slug of warm water moves across the surface from the relatively intensely heated shallows into the deeper regions where the heating/cooling is much less intense. This means that the slug of warm water remains at nearly
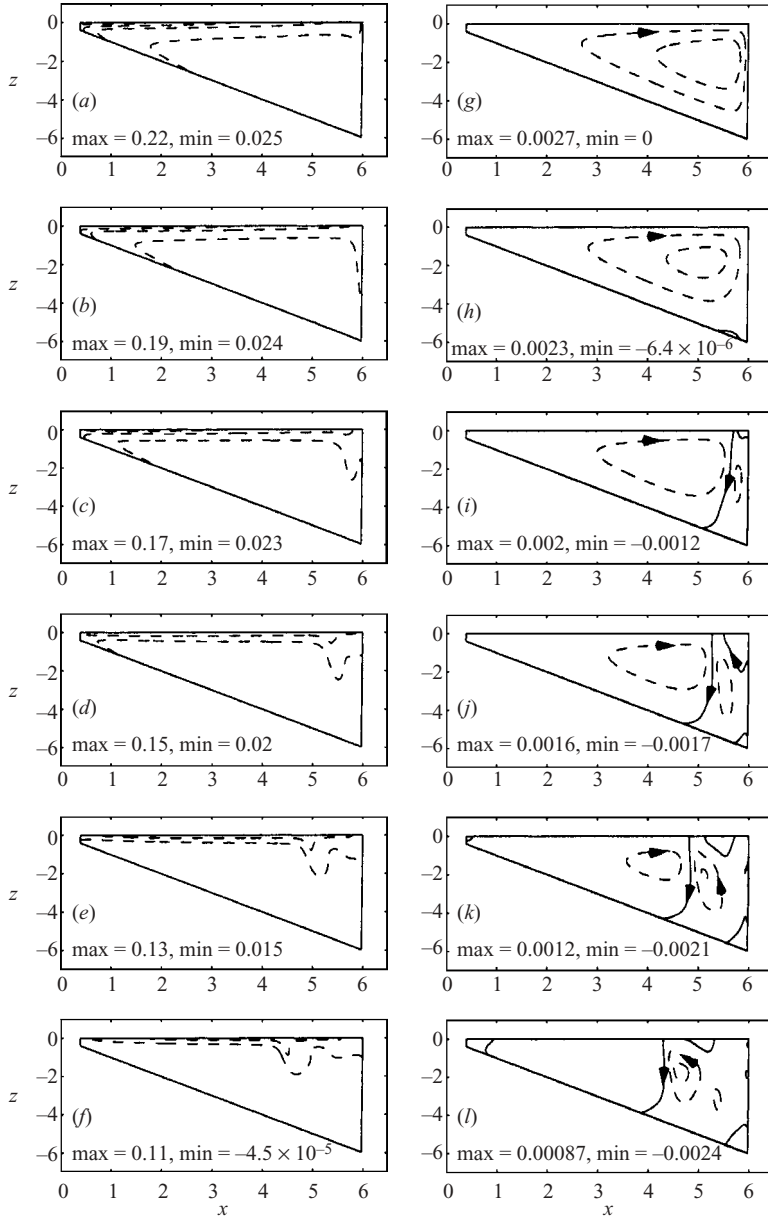
FIGURE 7. Series of snapshots of $(a–e)$ temperature and $(f–j)$ streamfunction from the asymptotic solution for $h = x$ at around the time that the warm surface current hits the endwall. The contour intervals are for $(a–e)$ 0.05 and for $(f–j)$ 0.001. Here, $A = 0.1$, $Gr = 10^6$, $r_{max} = 6$ and $\sigma = 7$. The solid contour is the zero contour. (a, g) $t = 0.275$; (b, h) $t = 0.3$; (c, i) $t = 0.325$; (d, j) $t = 0.35$; (e, k) $t = 0.375$; (f, l) $t = 0.4$.

the same temperature as it traverses the cavity. Eventually, the slug of warm water impacts the endwall in a manner similar to that observed in the differentially heated cavity (Patterson & Armfield 1990) or heated triangular cavity (Lei & Patterson 2002).

Figure 7 shows a number of snapshots of the temperature and streamfunction from the numerical results for $A = 0.1$, $Gr = 10^6$ and $r_{max} = 6$ around the time that the

warm surface flow arrives at the endwall at $r_{max} = 6$ (which occurs at $t \approx 0.28$). Note that for the linear response discussed above there is a daytime temperature structure until $t = 0.5$. Thus warm water continues to leave the shallows after the initial ejection and forms a thin and warm surface layer (figure 7a). Shortly after the warm fluid has been carried down the endwall by the general circulation (figure 7b) its buoyancy generates a reversal in the circulation at the endwall (figure 7c,i). This reversal then propagates as an internal wave back towards the shallows (figure 7d–f, j–l). Since heat is carried away from the shallows in the surface flow the cooling in the shallows leads to an earlier reversal of the horizontal pressure gradient than occurs in the linear regime. This is evident in figure 7(l) ($t = 0.4$) where there is a small cell with an anticlockwise circulation near the shallow end of the cavity. In the linear regime this reversal does not occur until $t = 0.5$. The reversal of the horizontal temperature gradient in the shallows can be seen in figure 7(f).

The next significant event is the ejection of a cold slug of fluid from the shallows which then travels as a gravity current down the sloping bottom. Figure 8 shows a number of snapshots of the temperature and streamfunction as the gravity current travels through the cavity. Note that the initial reversal of daytime pattern occurred in the shallows at $t \approx 0.4$. The gravity current travels down the sloping bottom in a similar way to the warm surface fluid mentioned above. However, the cold fluid travels more quickly despite the temperature anomaly being approximately the same as for the warm surface flow. This is because the cold fluid is losing potential energy as it travels down the slope. The steepening gradients of the streamfunction near the bottom boundary evident in figure 8(g–i) indicate that the gravity current accelerates as it travels down the slope. When the gravity current arrives at the endwall it is turned upward. The subsequent flow in the end region is significantly more vigorous than the corresponding flow when the warm surface current reaches the endwall. The upflow in the end region is sufficiently strong for cold fluid in the gravity current to reach the surface (figure 8f). In a similar way to the warm surface flow, the cold bottom flow leads to a stratification near the bottom (figure 8f). The gravity current hitting the endwall also leads to internal waves propagating back towards the tip.

Both the warm surface flow and cold bottom flow lead to a permanently stratified interior which supports internal wave activity during the diurnal cycle. During each cycle new surface and bottom flows strengthen and maintain the stratification. The stratification is established in the deeper parts by the cavity 'filling up' with fluid ejected from the tip. This is similar to the filling process for a differentially heated cavity (Patterson & Imberger 1980). Eventually, the system reaches a balance where the warm/cold fluid generated in the shallows during each cycle barely has enough buoyancy anomaly to travel into the deeper parts of the cavity. The flow is sufficient to maintain rather than strengthen the stratification. At this time, the deep region of the cavity has a permanent stratification of fixed (in non-dimensional variables) strength. This is similar to one of the possible steady states for a differentially heated rectangular cavity described by Patterson & Imberger (1980). The steady state consists of a stratified interior with the stratification maintained by warm and cold fluid ejected from the vertical boundary layers.

For the present case, the timescale for the setting up of the stratified deep region depends on the size of the cavity and the nonlinearity parameter $A^2 Gr$. A crude estimate of this timescale can be calculated by considering the volume of fluid ejected from the shallows during one nighttime cycle and using this to estimate a filling time for the deep part of the domain. From the asymptotic solution, the maximum (non-dimensional) velocity is approximately 4×10^{-3} and this occurs at $x \approx 2$. The
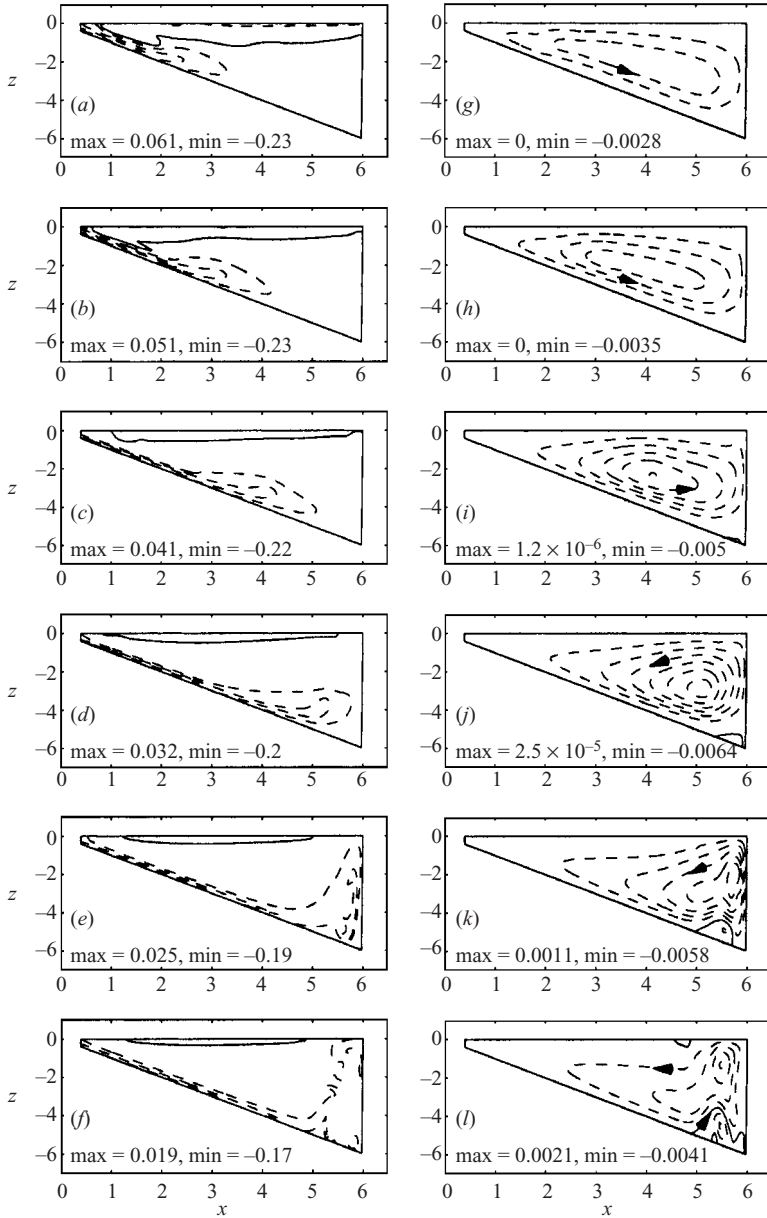
FIGURE 8. Series of snapshots of $(a\text{–}e)$ temperature and $(f\text{–}j)$ streamfunction from the asymptotic solution for $h = x$ showing the cold gravity current flowing down the slope. The contour intervals are for $(a\text{–}e)$ 0.05 and for $(f\text{–}j)$ 0.001. The parameters are as for figure 7. The solid contour is the zero contour. (a, g) $t = 0.55$; (b, h) $t = 0.575$; (c, i) $t = 0.6$; (d, j) $t = 0.625$; (e, k) $t = 0.65$; (f, l) $t = 0.675$.

volume of fluid ejected by the shallows over one nighttime cycle is then approximately $2 \times 10^{-3} A^2 Gr$. Half the volume of the cavity is approximately $r_{max}^2/4$. Thus the time taken for the stratification to form in the deep region due to this filling box process is $t_{fill} = 125 r_{max}^2 / A^2 Gr$.

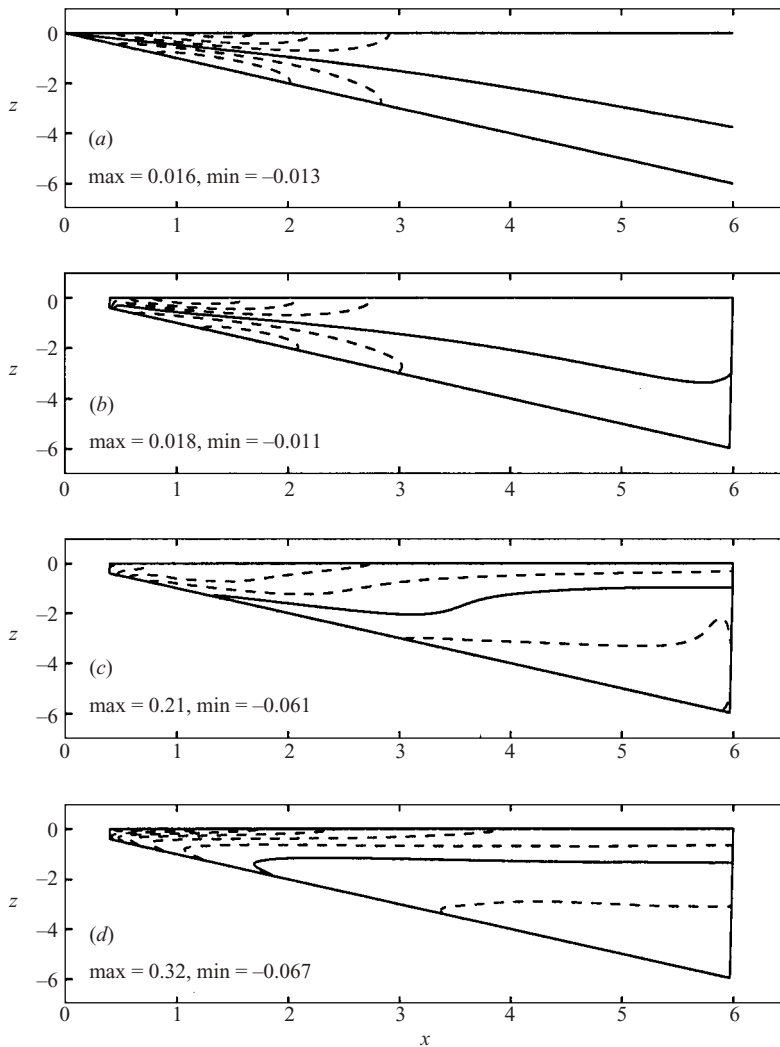FIGURE 9. Snapshots of the temperature field at $t = 8$ with $A = 0.1$, $r_{max} = 6$ and $\sigma = 7$ from (a) asymptotic results with $Gr = 10^4$, (b) numerical results with $Gr = 10^4$, (c) numerical results with $Gr = 10^5$ and (d) numerical results with $Gr = 10^6$. The contour intervals are for (a, b) 0.005 and for (c, d) 0.05.

Figure 9 shows temperature contours at $t = 8$ from the asymptotic and numerical results for different values of Gr for $A = 0.1$ and $r_{max} = 6$. At $t = 8$ the average temperature in the cavity is zero. Figures 9(a) and 9(b) are for $Gr = 10^4$ from the asymptotic and numerical results respectively. For $Gr = 10^4$, $t_{fill} = 45$ which is much longer than $t = 8$. Note that the stratification process discussed above is cumulative over successive diurnal cycles. For example, cool water carried out from the shallows moves into a region where the heating/cooling and circulation is less intense. This means that over the course of a diurnal cycle the reversed flow will not carry it back into the shallows. This hysteresis effect is not captured by the $O(A^2)$ temperature which is purely periodic. In figure 9(a) the temperature structure is close to symmetrical about the zero contour. This is in contrast to figure 9(b) from the numerical results where there is a clear asymmetry about the zero contour since the cold bottom

Run	A	Gr	$A^2 Gr$	r_{max}	t_{fill}	ΔT
1	0.1	10^5	1×10^3	6	4.5	0.1017
2	0.1	10^6	1×10^4	6	0.45	0.1458
3	0.02	2.5×10^6	1×10^3	6	4.5	0.1017
4	0.25	10^5	6.25×10^3	6	0.72	0.1615
5	0.25	2×10^4	1.25×10^3	6	3.6	0.1485
6	0.1	10^6	1×10^4	4	0.2	0.1234
7	0.1	10^6	1×10^4	8	0.8	0.1524

TABLE 1. Summary of stratification strength at $t = 8$ from the numerical results for various parameters. For the last column, ΔT is the top to bottom temperature difference at $r = r_{max}$.

current is generally stronger than the warm surface current. Figure 9(c) shows the temperature structure at $t = 8$ from the numerical results for $Gr = 10^5$ for which $t_{fill} = 4.5$. Here, the stratification in the deeper parts has been established; however there is still some basin-scale internal wave activity associated with the warm and cold currents emanating from the shallows. Figure 9(d) shows the temperature structure at $t = 8$ for $Gr = 10^6$ for which $t_{fill} = 0.45$. Here, the stratification establishes in a time comparable to the diurnal period. By $t = 8$ the internal wave activity evident in figures 7 and 8 has died away and there is very little motion in the deep part of the cavity. In fact, the temperature field in the deep part of the cavity is close to steady with a barely perceptible change during the diurnal cycle.

Note that the (dimensionless) temperature difference from top to bottom in the deep part of the cavity is nearly the same for figures 9(c) and 9(d) despite the order of magnitude difference in Gr. This is because the strength of the stratification is set by the temperature of the fluid ejected from the tip during the diurnal cycle. Table 1 summarizes the vertical temperature difference at $t = 8$ in the deep part of the cavity for a range of values for A, Gr and r_{max}. All simulations have $t_{fill} < 8$. The vertical temperature difference ranges from 0.1017 to 0.1615. The smaller number corresponds to cases where $t_{fill} = 4.5$ (Runs 1 and 3). A closer examination of these runs shows that there is still some basin-scale internal wave activity at $t = 8$ so the stratification in the deep regions has not yet settled down. Ignoring those two runs, the average ΔT is 0.1463 with all values being within 26% of this value despite the much larger variation in the input parameters. This reinforces the result that the long-term stratification strength in the deep part of the domain depends primarily on the behaviour in the shallows.

These results can be used to estimate the deep-region stratification strength in natural lakes due to this process. Using $I_0 = 10^3 \, \text{W m}^{-2}$ and the usual values for the other parameters gives ΔT ranging from 10 °C for molecular values for ν to 1 °C for an eddy viscosity of $\nu = 10^{-4} \, \text{m}^2 \, \text{s}^{-1}$. The observations of Monismith et al. (1990) show a semi-permanent stratification in a reservoir sidearm of 2 °C or 3 °C which is consistent with the present results. The corresponding circulation velocities range from $\sim 1 \, \text{cm s}^{-1}$ to $\sim 10 \, \text{cm s}^{-1}$ which is also consistent with the field observations of Monismith et al. (1990). It is difficult to have a more detailed comparison since the field results are influenced by wind and more complicated heating/cooling mechanisms.

6. Conclusions

This paper has formulated a model for periodically (in time) forced natural convection of a fluid over varying bathymetry. This models the diurnal heating/cooling

cycle in lakes with differential heating/cooling associated with variable depth. The model is analysed using asymptotic methods based on a small characteristic bottom slope and numerically using a SIMPLE type algorithm for a particular geometry. The asymptotic results provide an adequate description of the flow so long as the degree of nonlinearity in the dynamics is weak. In this case, the flow response consists of viscous-dominated flow in the shallows with the flow response being in phase with the forcing and an unsteady inertia-dominated flow in the deeper parts where the response lags the forcing. The characteristics of these two regions is captured by two limiting cases of the model. The asymptotic results predict a relatively weak stable thermal stratification set up by advection and this prediction is borne out by the numerical solution of the full equations for the weakly nonlinear case.

When nonlinear effects become stronger the presence of vertical boundaries has a significant effect on the flow. In particular, for the triangular geometry, surface and gravity currents emanating from the shallow regions are stopped from travelling to infinity and eventually pool in the deeper parts of the domain. The resultant stable stratification can support internal wave activity generated by gravity and surface currents hitting the endwall. Eventually, the stratification reaches a maximum strength and (in terms of the non-dimensional variables) this is largely independent of both the size of the domain and the degree of nonlinearity. The timescale for the setting up of the stratification decreases as nonlinear effects increase in importance and can be less than the period of the forcing.

There are a number of avenues for further work, especially additional numerical modelling. The modelling here is for one particular geometry. It would be interesting to investigate more general geometries numerically in the nonlinear regime to further examine the stratification process for unsteady forcing. There is also the issue of using open boundary conditions. It was mentioned in §2 that the vertically uniform heating/cooling is a simplification of the mechanisms operating in natural lakes. Although the daytime heating and nighttime cooling scenarios have been separately considered, there appears to be no analytical or numerical investigation of a more realistic combined model for the diurnal heating/cooling cycle. Finally, the simulations reported here are for Gr at the lower end of values for natural lakes. Examination of the flow for higher Gr is necessary for a more detailed comparison to natural lakes.

Appendix. The second-order temperature $T^{(2)}$

To facilitate the solution, $T^{(2)}$ is written as $T^{(2)} = T^{(2)}_{\text{cond}} + T^{(2)}_{\text{adv}}$ where $T^{(2)}_{\text{cond}}$ is the correction due to horizontal conduction and proper matching of the lower boundary condition and $T^{(2)}_{\text{adv}}$ is the correction due to advection. The conduction solution is

$$T^{(2)}_{\text{cond}} = \frac{1 - \cos(2\pi t)}{4\pi^2 \sigma h^3}(h'^2 - hh'') - \frac{h'^2}{\pi h^3}\sum_{n=1}^{\infty}(-1)^n \cos\left(\frac{n\pi z}{h}\right)$$

$$\times \frac{(n\pi/h)^2 \sin(2\pi t) + 2\pi\sigma\left[\exp(-(n\pi/h)^2 t/\sigma) - \cos(2\pi t)\right]}{(n\pi/h)^2 + (2\pi\sigma)^2}. \quad \text{(A 1)}$$

The advection solution can be written as

$$T_{\text{adv}}^{(2)} = Gr\sigma h h'^2 \sum_{m=1}^{\infty} a_m(t) \left(\cos \frac{m\pi z}{h} \right) \tag{A 2}$$

where

$$a_m(t) = \frac{8(1-(-1)^m)+(-1)^m(m\pi)^2}{4\pi^2(m\pi)^6(m^4\pi^2+16h^4\sigma^2)}$$

$$\times \left[\frac{m^4\pi^2}{8}(1-\cos(4\pi t)) - \frac{1}{2}\pi h^2\sigma m^2 \sin(4\pi t) + 2h^4\sigma^2\left(1-\mathrm{e}^{-(m\pi/h)^2 t/\sigma}\right) \right]$$

$$+ \frac{4(-1)^m}{\pi} \sum_{n=1}^{\infty} \frac{\cos\beta_n + (\cos\beta_n - 1)/\beta_n^2 - \frac{1}{2}}{\beta_n^2\left((m\pi)^2 - \beta_n^2\right)\left((\beta_n/h)^4 + 4\pi^2\right)} b_{mn}(t) \tag{A 3}$$

where

$$b_{mn}(t) = \left(\frac{\beta_n}{h}\right)^2 \left(\frac{h^2\sigma\left(\mathrm{e}^{-(m\pi/h)^2 t/\sigma} - \cos(4\pi t)\right) + \frac{1}{4}m^2\pi\sin(4\pi t)}{\pi(m^4\pi^2 + 16h^4\sigma^2)} \right.$$

$$\left. - \frac{\pi h^2\sigma\left(\mathrm{e}^{-(m\pi/h)^2 t/\sigma} - \mathrm{e}^{-(\beta_n/h)^2 t}\cos(2\pi t)\right) + \frac{1}{2}\left(m^2\pi^2 - \beta_n^2\sigma\right)\mathrm{e}^{-(\beta_n/h)^2 t}\sin(2\pi t)}{\left((m\pi)^2 - \beta_n^2\sigma\right)^2 + 4\pi^2 h^4\sigma^2} \right)$$

$$- \pi \frac{\frac{1}{2}m^4\pi^2(\cos(4\pi t) - 1) + 2\pi h^2\sigma m^2\sin(4\pi t) + 8h^4\sigma^2\left(\mathrm{e}^{-(m\pi/h)^2 t/\sigma} - 1\right)}{(m\pi)^2(m^4\pi^2 + 16h^4\sigma^2)}. \tag{A 4}$$

Note that $T_{\text{adv}}^{(2)}$ includes terms proportional to $\cos(4\pi t)$ and $\sin(4\pi t)$ which arise from the nonlinear combination of longer-period terms in the forcing.

REFERENCES

ADAMS, E. E. & WELLS, S. A. 1984 Field measurements on side arms of Lake Anna, Va. *J. Hydraul. Engng* **110**, 773–793.

ARMFIELD, S. W. 1991 Finite-difference solutions of the Navier-Stokes equations on staggered and non-staggered grids. *Computers Fluids* **20**, 1–17.

CORMACK, D. E., LEAL, L. G. & IMBERGER, J. 1974 Natural convection in a shallow cavity with differentially heated end walls. Part 1. Asymptotic theory. *J. Fluid Mech.* **65**, 209–229.

CORMACK, D. E., STONE, G. P. & LEAL, L. G. 1975 The effect of upper surface conditions on convection in a shallow cavity with differentially heated end-walls. *Intl J. Heat Mass Transfer* **18**, 635–648.

FARROW, D. E. 1995 A numerical model of the hydrodynamics of the thermal bar. *J. Fluid Mech.* **303**, 279–295.

FARROW, D. E. & PATTERSON, J. C. 1993 On the response of a reservoir sidearm to diurnal heating and cooling. *J. Fluid Mech.* **246**, 143–161 (referred to herein as FP93).

FARROW, D. E. & PATTERSON, J. C. 1994 The daytime circulation and temperature pattern in a reservoir sidearm. *Intl J. Heat Mass Transfer* **37**, 1957–1968.

HART, J. E. 1972 Stability of thin non-rotating Hadley circulations. *J. Atmos. Sci.* **29**, 687–697.

HORSCH, G. M., STEFAN, H. G. & GAVALI, S. 1994 Numerical-simulation of cooling-induced convective currents on a littoral slope. *Intl J. Num. Meth. Fluids* **19**, 105–134.

LEI, C. & PATTERSON, J. C. 2002 Unsteady natural convection in a triangular enclosure induced by the absorption of radiation. *J. Fluid Mech.* **460**, 181–209.

LEONARD, B. P. 1979 A stable and accurate convective modelling procedure based on quadratic upstream interpolation. *Comput. Meth. Appl. Mech. Engng* **19**, 59–98.

MONISMITH, S. G., IMBERGER, J. & MORISON, M. L. 1990 Convective motions in the sidearm of a small reservoir. *Limnol. Oceanogr.* **35**, 1676–1702.

PATTERSON, J. C. & ARMFIELD, S. W. 1990 Transient features of natural convection in a cavity. *J. Fluid Mech.* **219**, 469–497.

PATTERSON, J. C. & IMBERGER, J. 1980 Unsteady natural convection in a rectangular cavity. *J. Fluid Mech.* **100**, 65–86.

POULIKAKOS, D. & BEJAN, A. 1983 The fluid mechanics of an attic space. *J. Fluid Mech.* **131**, 251–269.

RATTRAY, M., JR. & HANSEN, D. V. 1962 A similarity solution for circulation in an estuary. *J. Mar. Res.* **20**, 121–133.

STURMAN, J. J., OLDHAM, C. E. & IVEY, G. N. 1999 Steady convective exchange flow down slopes. *Aquat. Sci.* **61**, 260–278.